Icarus **159**, 284–299 (2002)
doi:10.1006/icar.2002.6927

Stable Chaos versus Kirkwood Gaps in the Asteroid Belt: A Comparative Study of Mean Motion Resonances

Kleomenis Tsiganis, Harry Varvoglis, and John D. Hadjidemetriou

Section of Astrophysics, Astronomy and Mechanics, Department of Physics, University of Thessaloniki, 54124 Thessaloniki, Greece
E-mail: tsiganis@astro.auth.gr

Received September 14, 2001; revised March 29, 2002

We have shown, in previous publications, that *stable chaos* is associated with medium/high-order mean motion resonances with Jupiter, for which there exist no resonant periodic orbits in the framework of the elliptic restricted three-body problem. This topological "defect" results in the absence of the most efficient mechanism of eccentricity transport (i.e., large-amplitude modulation on a short time scale) in three-body models. Thus, chaotic diffusion of the orbital elements can be quite slow, while there can also exist a nonnegligible set of chaotic orbits which are semiconfined (stable chaos) by "quasi-barriers" in the phase space. In the present paper we extend our study to all mean motion resonances of order $q \leq 9$ in the inner main belt (1.9–3.3 AU) and $q \leq 7$ in the outer belt (3.3–3.9 AU). We find that, out of the 34 resonances studied, only 8 possess resonant periodic orbits that are continued from the circular to the elliptic three-body problem (regular families), namely, the 2/1, 3/1, 4/1, and 5/2 in the inner belt and the 7/4, 5/3, 11/7, and 3/2 in the outer belt. Numerical results indicate that the 7/3 resonance also carries periodic orbits but, unlike the aforementioned resonances, 7/3-periodic orbits belong to an irregular family. Note that the five inner-belt resonances that carry periodic orbits correspond to the location of the main Kirkwood gaps, while the three outer-belt resonances correspond to gaps in the distribution of outer-belt asteroids noted by Holman and Murray (1996, *Astron. J.* 112, 1278–1293), except for the 3/2 case where the Hildas reside. Fast, intermittent eccentricity increase is found in resonances possessing periodic orbits. In the remaining resonances the time-averaged elements of chaotic orbits are, in general, quite stable, at least for times $t \sim 250$ Myr. This slow diffusion picture does not change qualitatively, even if more perturbing planets are included in the model. © 2002 Elsevier Science (USA)

Key Words: asteroids, dynamics; celestial mechanics; chaos.

1. INTRODUCTION

Recent studies have shown that a large number of real asteroids follow chaotic trajectories (see Knežević and Milani 2000). Chaos can force asteroids to develop planet-crossing orbits and suffer repeated close encounters with the major planets, eventually being driven away from the main belt. The macroscopic results of this process are imprinted in the orbital distribution of asteroids, the most prominent features being the *Kirkwood gaps*, associated with the low-order mean motion resonances with Jupiter, namely, the 2/1, 3/1, 4/1, 5/2, and 7/3 resonances (see Moons 1997 for a review on the dynamics). Apart from the inner-belt gaps, Holman and Murray (1996) noted that the distribution of semi-major axes of outer-belt (beyond 3.3 AU) asteroids also presents gaps, the most prominent ones being related to the 5/3, 7/4, and 8/5 mean motion resonances.

On the other hand, chaos does not always lead to a rapid growth of eccentricity. During the past decade many authors have found strongly chaotic orbits, in terms of Lyapunov exponents, which do not show significant variations of their elements for times much longer than the Lyapunov time. Such "slow" chaos can be found within wide domains of the phase space. Milani and Nobili (1992) introduced the terminology *stable chaos*, to emphasize the paradoxal motion of the asteroid (522) Helga, which resides in the vicinity of the 12/7 mean motion resonance with Jupiter ($a \approx 3.63$ AU). Its orbit is very chaotic (Lyapunov time $T_L \sim 7000$ years), but, the proper values of its semi-major axis, a, eccentricity, e, and inclination, i, are very stable for times longer than $10^3\, T_L$. The motion of Helga was also studied by Holman and Murray (1996) and in more detail by Tsiganis *et al.* (2000), who both found that its orbital elements do not change significantly for times of $\sim 10^9$ years. Subsequently, many more cases of real asteroids exhibiting this kind of motion were found (see, e.g., Milani *et al.* 1997, Šidlichovský 1999). In Tsiganis *et al.* (2000, 2002) we noted that the orbit of Helga, as well as of other real asteroids exhibiting stable chaos, also has a property that leads to a distinction between "slow" and "stable" chaos. This property is that not only do the variations of e and i have a very small amplitude (this is common in both types of chaotic motion), but also the "jumps" Δe and Δi are very well correlated for times longer than $10^3\, T_L$. This implies that the associated proper frequencies are almost constant with time. In this respect the word "stable" does not refer to stability in the sense of Lyapunov, but rather it describes an orbital behavior where the elements seem to evolve in a nearly quasi-periodic manner for times much greater than T_L.

0019-1035/02 $35.00

The following question remains to be answered now: Why is there only a small number of gaps in the distribution of asteroids, while chaotic motion seems to be the rule, rather than the exception, in numerical integrations? Obviously the answer can only be obtained by analyzing the various chaos-generating mechanisms, the associated transport process, and the relevant time scales. In the next section we will briefly review these mechanisms and describe their main effects.

2. DYNAMICAL MECHANISMS LEADING TO CHAOS

Chaos in the main belt results from *resonances* between the unperturbed frequencies of motion of an asteroid and the driving frequencies of the system, the latter being (a) the frequencies of revolution of the main perturbing planets (especially Jupiter) and (b) the frequencies of precession of the planetary orbits. Resonances between the revolution frequency (mean motion, n) of an asteroid and that of a planet (n'; most usually Jupiter) are referred to as *mean motion resonances*. These are defined by the condition $p\dot{\lambda} + q\dot{\lambda}' = pn + qn' \approx 0$, where λ (resp. λ') denotes the mean longitude of the asteroid (resp. Jupiter) and p, q are integers. In the three-body problem (Sun–Jupiter–asteroid) only this type of resonance occurs, since n' is the only nonzero driving frequency.[1] If the orbit of the perturber is allowed to precess, or more perturbing planets are taken into account, mean motion resonances are forced to pulsate. More important *secular resonances* between the frequencies $g = \langle \dot{\varpi} \rangle$ and $s = \langle \dot{\Omega} \rangle$ of the asteroid and the fundamental secular frequencies of the planetary system, g_i and s_i, are possible. The associated critical arguments are of the form $k\varpi + p\Omega + \sum_i (q_i \varpi_i + r_i \Omega_i)$, where ϖ_i and Ω_i are linear approximations of the planetary arguments and k, p, q_i, r_i are integers. Note that, for both types of resonance, the integers involved must obey a set of relations, known as the *D'Alembert rules*.

Secular resonances can greatly modulate an asteroid's eccentricity and/or inclination. Analytic and synthetic secular theories, derived by many authors (see, e.g., Bretagnon 1974, Nobili *et al.* 1989, Laskar 1990, Knežević *et al.* 1991), can help in computing the location of secular resonances *outside* mean motion resonances. First-order secular resonances bound the distribution of main-belt asteroids in the (a, i) space (see, e.g., Michel *et al.* 2000). Also, the unrealistically wide (in the frame of a three-body model) gap associated with the 4/1 resonance is explained by the presence of the ν_6 ($\langle \dot{\varpi} \rangle \approx g_6$) and ν_{16} ($\langle \dot{\Omega} \rangle \approx s_6$) secular resonances at $a \approx 2$ AU ($i \leq 5^\circ$). However, secular resonances can also occur *inside* the libration zone of a mean motion resonance, as the latter can significantly modify the values of the secular frequencies, with respect to their unperturbed values. In fact, although numerous chaotic orbits can be found in mean motion resonances, complete depletion of these regions does not occur in the three-body problem. The overlap of coexisting secular resonances destroys the stability islands and leads to large-scale eccentricity transport, within relatively short time scales (Moons and Morbidelli 1995). Finally, when the direct effects of more than one planet are taken into account, *three-body mean motion resonances* appear (Nesvorný and Morbidelli 1998a, Murray *et al.* 1998). A resonance of the Jupiter–Saturn–asteroid type occurs when $p\dot{\lambda}_J + q\dot{\lambda}_S + r\dot{\lambda} \approx 0$. For a given degree in eccentricity these resonances are much more dense than ordinary mean motion resonances in the belt (although much weaker; see Nesvorný and Morbidelli 1998b), contributing significantly to chaotic diffusion in the belt.

In this paper we will focus on a comparative study of mean motion resonances with Jupiter. The main interest in this study comes from the fact that the phase-space topology induced by resonance may be very different from case to case. In the *elliptic* three-body problem a mean motion resonance splits into a multiplet of nearby (in frequency space) harmonics. If we only consider orbits that are co-planar with the perturber's orbit, each harmonic is identified by a different critical argument, of the form

$$\sigma_k = (p+q)\lambda' - p\lambda - q\varpi + k(\varpi - \varpi') = \sigma + k\phi. \quad (1)$$

The $k \neq 0$ terms represent resonances between the two slow angles, σ and ϕ, of the averaged problem, these are also called "secondary resonances." The harmonics may or *may not* have a common node in the (a, e) space, defined by $\dot{\phi} = 0$ (called "corotation resonance" by Henrard and Caranicolas 1990). This node appears as a pair of fixed points on the $(X = e\cos\phi, Y = e\sin\phi)$ surface of section of the averaged problem (see, e.g., Hadjidemetriou 1993), which correspond to the intersection of two resonant periodic orbits (one stable and one unstable) of the nonaveraged problem with the considered "energy" manifold. An island of libration of ϕ develops around the stable fixed point, and the homoclinic layer of the unstable periodic orbit encircles this island. This topological structure provides a very efficient mechanism for the growth of the eccentricity. Wandering of α chaotic trajectory around the island leads to $e \sim 0.9$ (for the 3/1 resonance) within half the libration period, with the eccentricity evolving in an intermittent manner, first seen by Wisdom (1982).

Even if resonant periodic orbits do not exist for a given orbital commensurability, chaos is still produced by the overlapping of the closely spaced resonant harmonics. The efficiency of this overlap depends on the width and mutual distance of the harmonics, which scale with e. Some resonant multiplets may generate global chaos in their vicinity while, for other cases, chaotic orbits can be semiconfined within thin layers in phase space (see Morbidelli and Guzzo 1997). Most outer-belt resonances (beyond 3.3 AU) are almost globally chaotic, with asteroids experiencing a slow diffusion in the space of proper elements, according to the analytic model of Murray and Holman (1997). On the other hand, in the resonances studied by Tsiganis *et al.* (2000, 2002), both slowly diffusing and stable-chaotic orbits were identified.

[1] The longitude of pericenter, ϖ', and the longitude of the node, Ω', of Jupiter are constant; i.e., $g' = \dot{\varpi}' = 0 = \dot{\Omega}' = s'$.

We begin our study by searching for periodic orbits inside different resonances (Section 3), in order to describe qualitatively the transport properties of chaotic orbits. Numerical results of orbital integrations of fictitious asteroids are presented in Section 4 and conclusions are given in Section 5.

3. SEARCHING FOR RESONANT PERIODIC ORBITS

We study all mean motion resonances with Jupiter, defined by the integer ratio $n/n' = (p+q)/p$, with $q \leq 9$ for the inner belt and $q \leq 7$ for the outer belt. The p's are selected so that $1.9 \leq a \leq 3.9$ AU. By adding the 3/2 resonance ($a \approx 3.96$ AU), where the Hildas reside, a total of 34 cases is considered. First, we compute the main families of resonant periodic orbits in the 2D circular restricted three-body problem (hereafter *circular problem*). Next, we examine whether these families continue (or not) in (i) the 2D elliptic restricted three-body problem (Jupiter on a fixed ellipse; hereafter *elliptic problem*) and (ii) the 3D circular restricted problem (hereafter *3D problem*).

3.1. Circular Problem

Let us assume Jupiter to move on a circular orbit around the Sun and consider a uniformly rotating frame of reference in the plane of motion, (x, y), the origin of which is at the center of mass of the two bodies and the x axis is on the Sun–Jupiter line. The unit of mass is the sum of the masses of the two bodies (μ is the ratio of Jupiter's mass to the total mass) and the unit of distance is the radius of Jupiter's orbit. By setting the gravitational constant $G = 1$, the period of Jupiter becomes $T_J = 2\pi$. It can be proved that, in this rotating frame, there exist families of periodic orbits of the massless body (asteroid) symmetric with respect to the x axis. We can distinguish between *circular* and *elliptic* families of periodic orbits. Along a circular family the eccentricity of the asteroid stays close to zero, but the semi-major axis and the mean motion vary. In contrast, along an elliptic family, the eccentricity of the asteroid increases from zero to unity, while the semi-major axis and the mean motion stay almost constant. In all cases of elliptic motion both stable and unstable orbits exist. We refer to Hadjidemetriou (1993) for a detailed discussion on this topic.

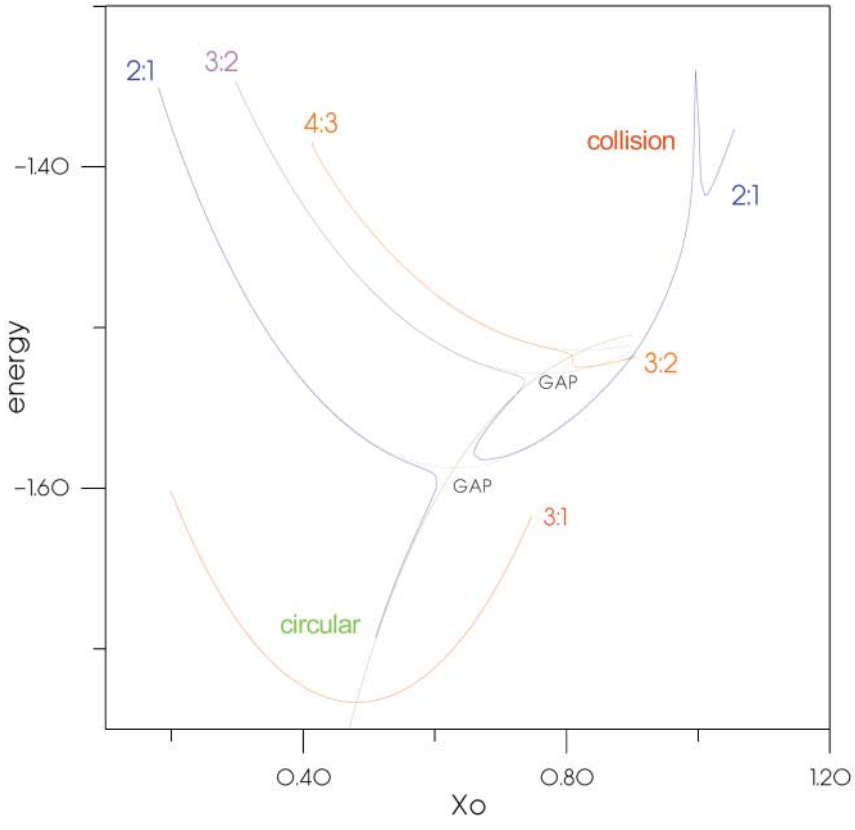

FIG. 1. Families of resonant periodic orbits (circular problem, $\mu = 0.000954786$) in the (x_0, energy) space. The curves shown here correspond to the circular family and the elliptic branches of the 3/1, 2/1, 3/2, and 4/3 resonances. The point of collision with Jupiter for 2/1 resonant orbits is also shown. Note that, for first-order resonances, the pericentric and apocentric branches do not join smoothly on the circular branch, in contrast to the 3/1 case, and "gaps" of elliptic periodic orbits appear. The extent of these gaps can be seen by superimposing the unperturbed ($\mu = 0$, dotted curves) families of periodic orbits. Instead, for $p/(p+1)$ resonances, the pericentric branch of the $p = k+1$ resonance (e.g., 4/3) is connected with the apocentric branch of the $p = k$ resonance (resp. 3/2) through a branch of circular periodic orbits. The deviation of these connecting circular branches from the unperturbed circular family becomes more evident as Jupiter is approached. Finally, elliptic branches of different resonances cannot intersect but may seem to do so, since the sign of $\dot{y}_0$ is not specified on the plot.

At each of the 34 resonances studied here there exists a family of resonant periodic orbits, symmetric with respect to the x axis. Any orbit of this family is uniquely determined by a point $(x_0,\ \dot{y}_0)$ in the $(x, \dot{y})$ space of initial conditions (with $y_0 = 0$ and $\dot{x}_0 = 0$). Thus, each family is represented by a continuous curve, the *characteristic curve*, in the $(x_0,\ \dot{y}_0)$ space. Instead, we can represent these families in the (x_0, *energy*) space, where by "energy" we denote the value of the Jacobi constant. Some of the above-mentioned families are shown in Fig. 1. Each elliptic family is composed of two branches: the *pericentric* one (asteroid initially at perihelion, $\varpi = 0$) and the *apocentric* one (asteroid initially at aphelion, $\varpi = \pi$). The specific shape of the curves depends on the value of μ. Figure 1 corresponds to the actual value of Jupiter's mass, $\mu = 0.000954786$.

3.2. Elliptic Problem

In the elliptic problem, families[2] of resonant $(p+q)/p$ periodic orbits can bifurcate from a point of the *elliptic branch* of the family of the circular problem, if the period is *exactly* equal to $T = p\,2\pi$. For a particular resonance, such bifurcation points may or may not exist. As can be seen in Table I[3] (some examples are shown in Fig. 2a) this condition is *not* fulfilled for most of the resonances studied here; the characteristic curves, in the $(x_0,\ T)$ space, *do not intersect* the $T = p\,2\pi$ line. The only resonances for which periodic orbits continue in the elliptic problem are the 2/1, 3/1, 4/1, and 5/2 in the inner belt and the 7/4, 5/3, 11/7, and 3/2 in the outer belt. Thus, most resonant multiplets do not have a secular node (i.e., an island of libration) and the most efficient mechanism of eccentricity transport is absent. In the inner belt, the only resonances possessing this property are those associated with the known Kirkwood gaps (except for the 7/3 case, which we will study in a separate section). In the outer belt, the 3/2 resonance (where the Hildas reside) and some of the resonances associated with the "gaps" noted by Holman and Murray (1996) also carry periodic orbits in the elliptic problem.

3.3. 3D Problem

The aforementioned analysis is restricted to co-planar orbits. A more complete analysis of the dynamics requires the study of the possible continuation of the families of periodic orbits in a 3D configuration space. This is done by adding to the equations of motion of the circular problem the z component and assessing the *vertical stability* of each 2D periodic orbit. The stability index is the trace of the monodromy matrix, $\mathbf{A}$, for infinitesimally small displacements along the z direction. A 2D periodic orbit is said to be vertically stable if $|\mathrm{tr}(\mathbf{A})| < 2$; otherwise it is unstable. Periodic orbits for which $\mathrm{tr}(\mathbf{A}) = \pm 2$ are called *vertical critical orbits*, from which a family of 3D periodic orbits bifurcates. Performing these computations (see again Fig. 2a) we found that, again, most of the resonances studied do not posses vertical critical orbits. Continuation in the 3D problem occurs only for the 3/1, 2/1, 9/5, 5/3, and 3/2 resonances (see Fig. 2b). We note that the 3/1 and the 9/5 are "pathological cases" with respect to this kind of study. By this we mean that the stability index has steep variations, so that an accurate determination of the eccentricity of the bifurcation point is not easy (a question mark is placed in the corresponding cell of Table I). The 9/5 resonance is the only case for which continuation in the 3D problem but not in the elliptic problem occurs. As for the 7/3 case, we simply note here that 3D periodic orbits do not bifurcate from the plane, but still this is not the whole story.

TABLE I
Mean Motion Resonant Structure of the Asteroid Belt

$(p+q)/p$	a_{res} (AU)	$e' \neq 0$	$i \neq 0$	T_{L} (3BP)	Esc (3BP)	T_{L} (OSS)	Esc (OSS)
9/2	1.91	—	—	2.096	—	0.705	—
4/1	2.06	0.25	—	0.165	3/3	0.110	3/3
7/2	2.26	—	—	0.174	—	0.250	1/3
10/3	2.33	—	—	0.437	—	0.819	—
3/1	2.50	0.00, 0.80	?	0.076	3/3	0.068	3/3
11/4	2.65	—	—	0.835	—	1.345	—
8/3	2.70	—	—	0.145	—	0.121	—
5/2	2.82	0.15, 0.60	—	0.175	3/3	0.090	3/3
12/5	2.90	—	—	0.227	—	0.351	—
7/3	2.96	—	*	0.066	2/3	0.074	3/3
9/4	3.03	—	—	0.065	—	0.078	2/3
11/5	3.08	—	—	0.081	—	0.113	—
13/6	3.11	—	—	0.163	—	0.215	—
2/1	3.28	0.73	0.67, 0.80	0.029	2/3	0.064	3/3
11/6	3.47	—	—	0.032	1/3	0.040	2/3
9/5	3.52	—	0.46?	0.026	3/3	0.030	3/3
7/4	3.58	0.10, 0.36	—	0.015	3/3	0.009	3/3
12/7	3.63	—	—	0.037	—	0.068	—
5/3	3.70	0.00, 0.41	0.30, 0.40	0.014	3/3	0.017	3/3
13/8	3.76	—	—	0.135	—	0.137	—
8/5	3.80	—	—	0.012	3/3	0.041	3/3
11/7	3.85	0.02	—	0.026	1/3	0.029	2/3
3/2	3.97	0.46	0.39, 0.43	0.037	2/3	0.064	3/3

Note. Each resonance is indicated by the ratio n/n' (first column). The resonances are given in ascending order of their nominal locations, $a = a_{\mathrm{res}}$ (second column). The horizontal line marks the beginning of the outer belt. The next two columns show the value of e of the periodic orbit of the circular problem, which corresponds to the bifurcation point (if it exists) for the elliptic problem ($e' \neq 0$) and the 3D problem ($i \neq 0$). T_{L} is the Lyapunov time (in years if multiplied by 10^5) for an initial $e = 0.1$. "Esc" denotes the number of escapers from each resonance in the 3BP integration of RUN-II (sixth column). The last two columns are again T_{L} and "Esc," but for the OSS integration of RUN-II.

3.4. Summary

As shown here, the majority of mean motion resonances in the main belt (25/34 studied here) do not possess periodic orbits.

[2] These families are parametrized by the eccentricity of the perturber, e'.

[3] Only resonances with $q \leq 7$ for the inner belt and $q = 5$ for the outer belt are shown in Table I, since these are the cases for which a numerical study was also performed.

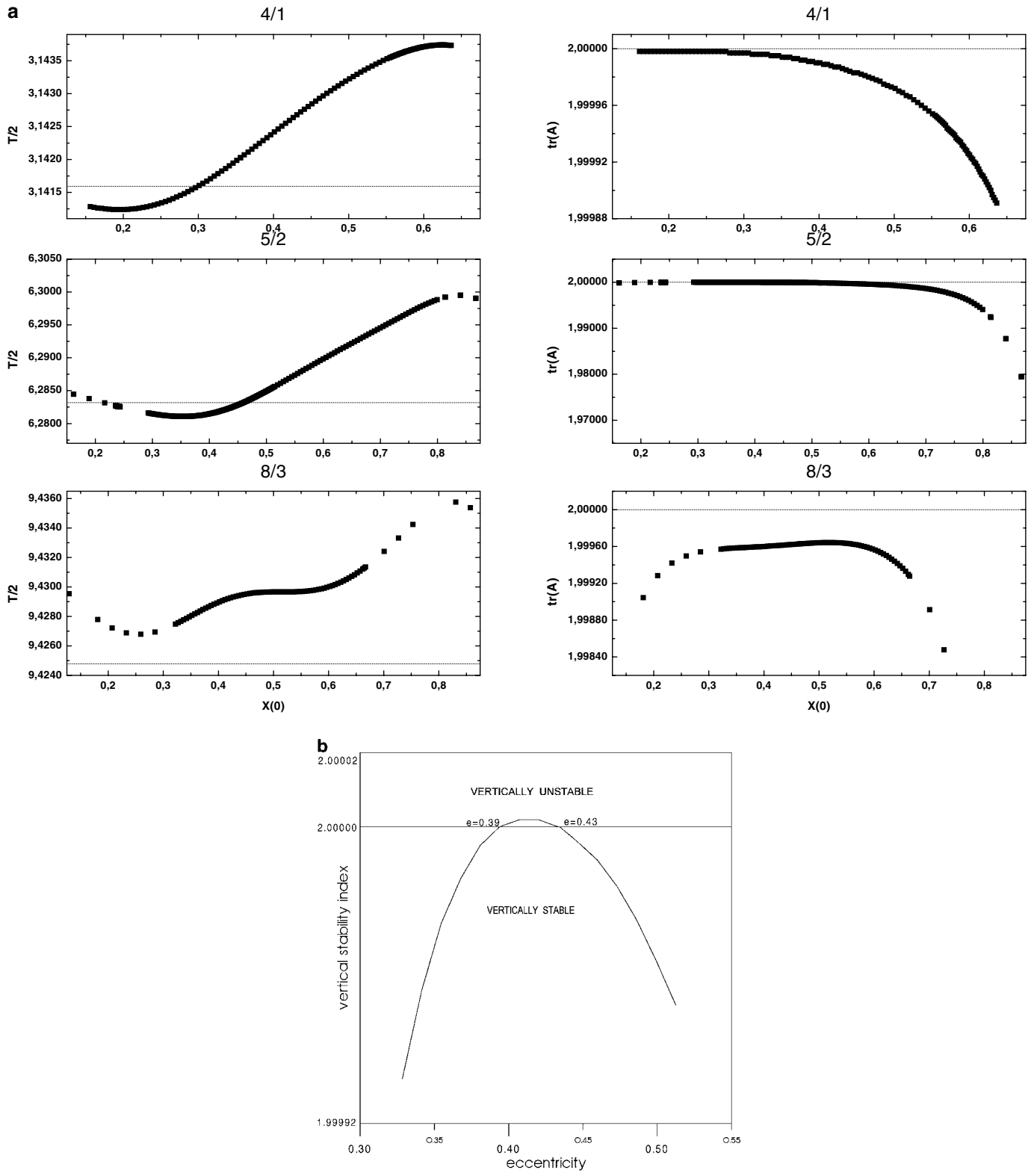

FIG. 2. (a) The half-period, $T/2$, of a resonant periodic orbit (left) and the trace of the monodromy matrix (right), tr($\mathbf{A}$), are graphically presented for the inner-belt resonances indicated on the plot. The bifurcation points for the elliptic problem are defined by the x_0 value for which $T/2 = p\pi$. The vertical critical orbits are located at the values of x_0 where tr($\mathbf{A}$) = 2. As can be seen on the plot, one bifurcation point for the elliptic problem and none for the 3D problem exist for the 4/1 resonance. Two bifurcation points for the elliptic and none for the 3D problem are found for the 5/2 resonance. In contrast, no bifurcation point exists for the 8/3 resonance. (b) The family of 3/2-resonant periodic orbits is shown as an example of vertical bifurcation. The x axis shows the eccentricity of the 2D periodic orbit (circular problem). Two vertical critical orbits (tr($\mathbf{A}$) = 2) are found at $e = 0.39$ and $e = 0.43$.

Thus, a slow—diffusive—evolution of chaotic orbits is expected. However, "semi confined" chaotic orbits may also exist, for which the only "escape" mechanism left (in the three-body framework) would be Arnol'd diffusion. In the remaining cases, which are the lowest order (i.e., stronger) ones, intermittent eccentricity transport is expected, due to the existence of libration islands. Including more planets in the model may change this picture, as described in Section 2. In the following section we check the validity of these propositions, with the aid of numerical integrations.

4. NUMERICAL INTEGRATIONS—RESONANT ORBITS

The orbits of a large number of test particles were numerically integrated to study the long-term evolution of chaotic orbits started in the vicinity of mean motion resonances. The initial conditions of the planets were taken from the Astronomical Almanac (2001, Epoch 2001 Feb 26.0) and were integrated for a short time, until Jupiter came to pericenter. Particles reaching $q = 0.005$ AU (Sun-grazers) or approaching a planet within a distance smaller than 1.5 Hill radii were "ejected" from the system. We used the MVS symplectic integrator (Wisdom and Holman 1991) implemented in the SWIFT package (Levison and Duncan 1994). The time step was set to $\tau = 10^{-2}\, T_{\rm J} \approx 43$ days, a compromise between accuracy[4] and computational cost. The integrations presented here sum up to several weeks of CPU time on a custom PC/Pentium III.

In our first numerical experiment (hereafter RUN-I) we scanned the "main belt" of the 3D elliptic three-body problem (hereafter 3BP), using sets of 280 test particles uniformly spread in a ($\Delta a = 0.005$, $2.0 \le a \le 3.4$ AU). Four such sets were used (1120 particles in total), each one being at a different initial eccentricity level, with $e = 0.05$, 0.1, 0.15, and 0.2 (i.e., all 280 particles in a set had the same initial value of e). The rest of the elements were given the values $i = 5^\circ$, $\varpi = \varpi_{\rm J}$, $\Omega = \Omega_{\rm J}$, and $\lambda = \lambda_{\rm J}$. Both the equations of motion and the variational equations (used for computing the maximal Lyapunov exponent) were solved for each particle. The objective of this experiment was to identify the main chaotic regions (resonances) of the inner belt and check the associated transport properties (intermittency vs diffusion) of chaotic trajectories for different values of e. A 2-Myr solution of the variational equations was first obtained (used for computing $T_{\rm L}$) and the orbits of those particles having $T_{\rm L} \le 2 \times 10^5$ years were subsequently integrated for 250 Myr.

The value of Δa chosen here can be larger than a high-order resonances' width, which, in the pendulum approximation, scales like $\delta\Lambda \sim \sqrt{\mu\, e^q}$ (for $e \approx e_{\rm J} \approx 0.05$), where $\Lambda = (\sqrt{a} - \sqrt{a_0})/k$ and a_0 is the nominal location of the resonance given by Kepler's law. To study chaotic motion in these thin resonances a second integration was performed (RUN-II), with particles initially placed inside the libration zone of each inner-belt (resp. outer-belt) resonance of order $q \le 7$ (resp. $q \le 5$). Three particles per resonance were integrated (all having the same values for i, ϖ, and Ω as before) at three different eccentricity values, $e = 0.05$, 0.01, and 0.15. The initial mean anomaly, M, was selected by setting the critical argument, $\sigma = p\,\lambda - (p+q)\,\lambda_{\rm J} + q\,\varpi$, equal to the value at which the center of libration of the resonance is located (circular problem), i.e., $\sigma = 0$ for odd q's and $\sigma = \pi$ for even q's. Finally, the initial values of a were chosen after performing a series of short-term numerical integrations, in which a was shifted by small amounts $\delta a \sim 10^{-2}$ AU with respect to a_0. In this way most of the selected particles were started in the chaotic zones of the respective resonances. While scanning the (thin in a) high-order resonances, we found several chaotic orbits (as shown by the behavior of the critical arguments) for each value of e. In most cases we could not detect a stability island (i.e., stable librations of σ) in the middle of the resonance, which means that chaos is the dominant behavior in high-order resonances. Thus, although a larger number of test particles would be desirable for a more refined analysis of the dynamics, we expect this set of few particles to be representative of the long-term evolution of chaotic orbits started inside high-order resonances. The variational equations for this set of 69 particles were integrated for 5 Myr, to enable detection of even larger values of $T_{\rm L}$ than in RUN-I. The equations of motion were solved for a time span of 250 Myr. Both the variational equations and the equation of motion were solved within two different models: (i) the 3BP model and (ii) the outer Solar System (hereafter OSS) model, in which the particle is subject to the (Newtonian) gravitational forces of the Sun and the four outer planets. The purpose of the OSS intergation was to check how the results of the 3BP model change when the effects of additional planets are present.

4.1. The Lyapunov Time

Let us denote by $v(t)$ the solution of the variational equations, i.e., the norm of the displacement vector tangent to the orbit, after time t. For chaotic orbits $v(t)$ grows exponentially with time and the limit $\gamma = \lim_{t\to\infty}\{\frac{1}{t}\ln[v(t)/v(0)]\}$ is the value of the maximal Lyapunov exponent. Its inverse, $T_{\rm L} = 1/\gamma$, is called the Lyapunov time. Having derived a 2-Myr (or 5-Myr) record for $v(t)$, an estimate of γ is obtained by a linear least-squares fit on $\ln v(t)$. Note that if $T_{\rm L} > 4 \times 10^5$ (or 10^6) years we cannot safely state that the orbit is chaotic, as a record of at least five times the actual value of $T_{\rm L}$ is needed for an accurate determination of γ through fitting.

Figure 3 shows graphically the results of RUN-I. It is evident that a small fraction of particles (from 7% for $e = 0.05$ to 10% for $e = 0.2$) follow chaotic trajectories. These are seen as dips in the distribution of $T_{\rm L}$. The upper bound of $T_{\rm L}$, which is indicated by the existence of a plateau in the graphs, reflects the short integration time. Chaotic orbits with very small values of $T_{\rm L}$ cannot be identified. A few peaks with $T_{\rm L}$ larger

[4] The accuracy of the MVS method is comparable to $\epsilon = \mathcal{O}(\mu\tau^2) \approx 10^{-7}$ for the Bulirsch–Stoer method. People using this integrator typically select τ between 20 (inner belt) and 80 (outer belt) days for long integrations ($t_{\rm int} > 100$ Myr).

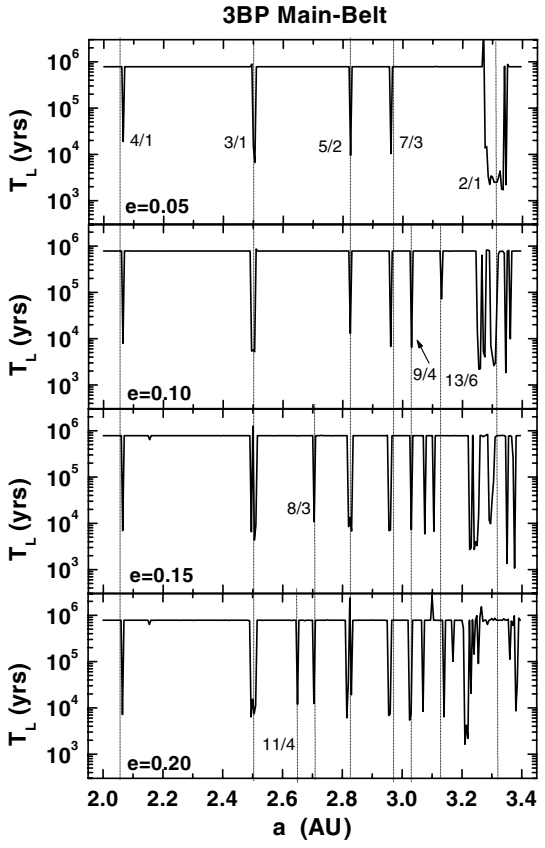

FIG. 3. The value of T_L is shown (in logarithmic scale) for each one of the 1120 particles of RUN-I. Each panel contains 280 values, corresponding to the 280 particles of each of the four sets. The initial eccentricity of the particles is also shown on each panel. The panels are in ascending order of e. For $e = 0.05$ one can identify only the 4/1, 3/1, 5/2, 7/3, and 2/1 resonances. As e grows to 0.2 more and more resonances become effective. The dotted vertical lines indicate the approximate location of the most important resonances, which are denoted by the value of $(p+q)/p$.

than the plateau value are also seen. These are an artifact of the fitting method and appear when a nearby chaotic zone induces large variations in the finite time series of $\ln v(t)$ of a regular orbit, which has a zero-slope secular trend. As noted on the figure, the initial value of a for these particles coincides with the location of the main mean motion resonances. For $e = 0.05$, chaotic trajectories are found only in the 4/1, 3/1, 5/2, 7/3, and 2/1 resonances. As the eccentricity is increased, more and more resonances are seen to generate chaos. For $e = 0.2$, most of the inner-belt resonances shown in Table I lead to chaotic motion, but the wide stability island of the 2/1 resonance also manifests itself.

Let us now take a deeper look at the high-order resonances. The results of RUN-II are shown in Fig. 4 (also Table I). Most of these particles follow chaotic orbits, both in the 3BP and the OSS integration. Only 5/69 particles in the 3BP and 2/69 in the OSS model, all starting at $e = 0.05$, seem to reside on regular orbits. Note that, as expected, the value of T_L continuously decreases as Jupiter is approached, as well as when the eccentricity is increased. Almost all chaotic orbits have $T_L \leq 10^5$ years and about half of them have $T_L \leq 10^4$ years, no matter what their initial eccentricity value. Note also that the differences between the 3BP and the OSS integration are minimal. This result implies that the degree of chaoticity of mean motion resonant orbits, as measured by T_L, is already determined by the three-body problem. However, the transport properties of this phase-space subset need not be preserved as well.

4.2. Long-Term Orbital Stability

In RUN-I a total of 90/1120 particles (8%) were found to follow chaotic orbits with $T_L \leq 2 \times 10^5$ years. These orbits were integrated for 250 Myr. Particles started in the gap resonances escaped from the belt (except from a few 2/1-resonant particles) either by encountering Jupiter or by developing effectively

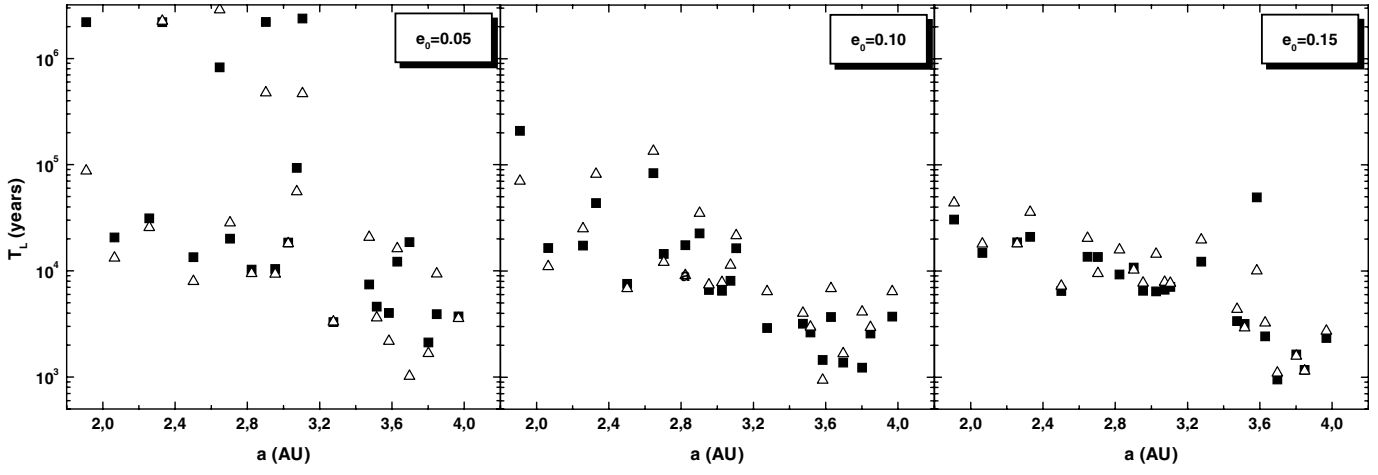

FIG. 4. The Lyapunov time $T_L = 1/\gamma$ (in years) for the particles of RUN-II is shown as a function of their initial value of semi-major axis, a_0. The y scale is logarithmic. The three panels correspond to the three different initial values of eccentricity, as indicated on the plot. The solid squares denote the particles of the 3BP integration while the empty triangles are those of the OSS integration.

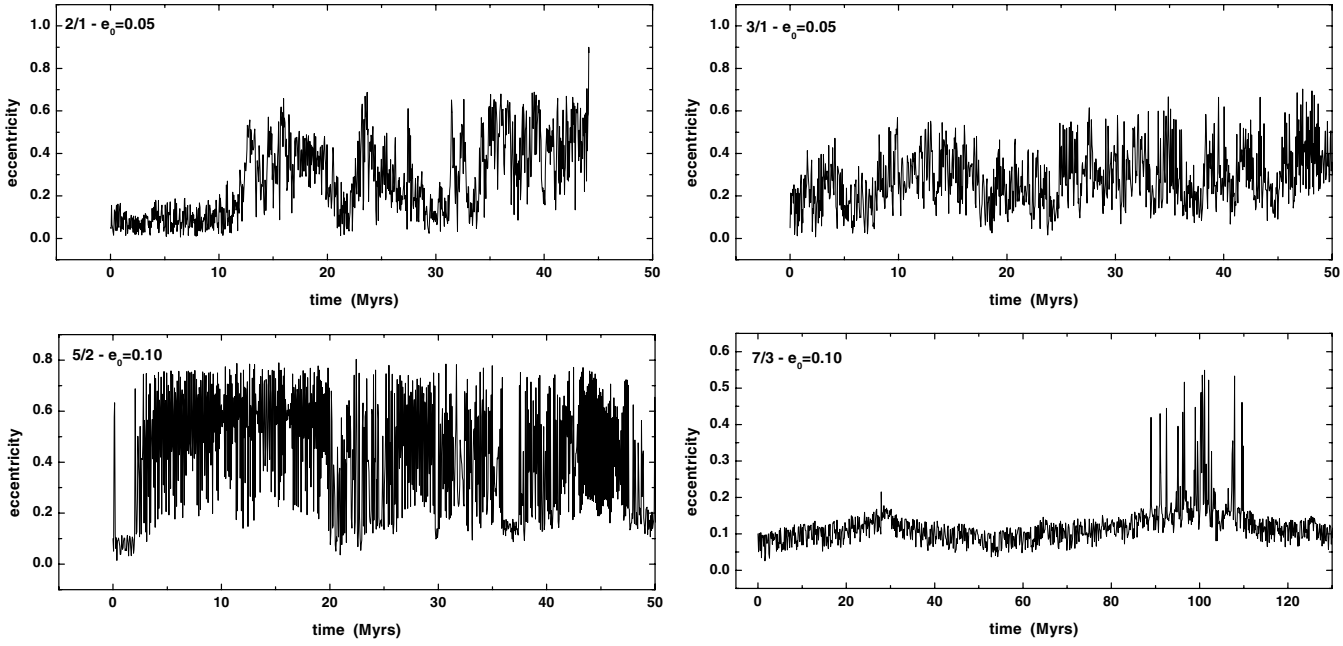

FIG. 5. The eccentricity evolution is shown for four RUN-I particles, started in the vicinity of the 2/1, 3/1, 5/2, and 7/3 resonances respectively. The initial eccentricity of each orbit is also shown in the plot. Large amplitude, intermittent, jumps in e, associated with the existence of resonant periodic orbits, are seen in all cases.

a Mars-crossing orbit. On the other hand, particles started at higher order resonances survived for the entire integration time span. Figures 5 and 6 show the time evolution of the eccentricity of some selected resonant particles. According to the results presented in Section 3, low-order resonances that carry periodic orbits induce intermittent jumps in e, leading particles to planet-crossing orbits. Conversely, in resonances that do not have periodic orbits, a slow diffusion of e is found and the time scale

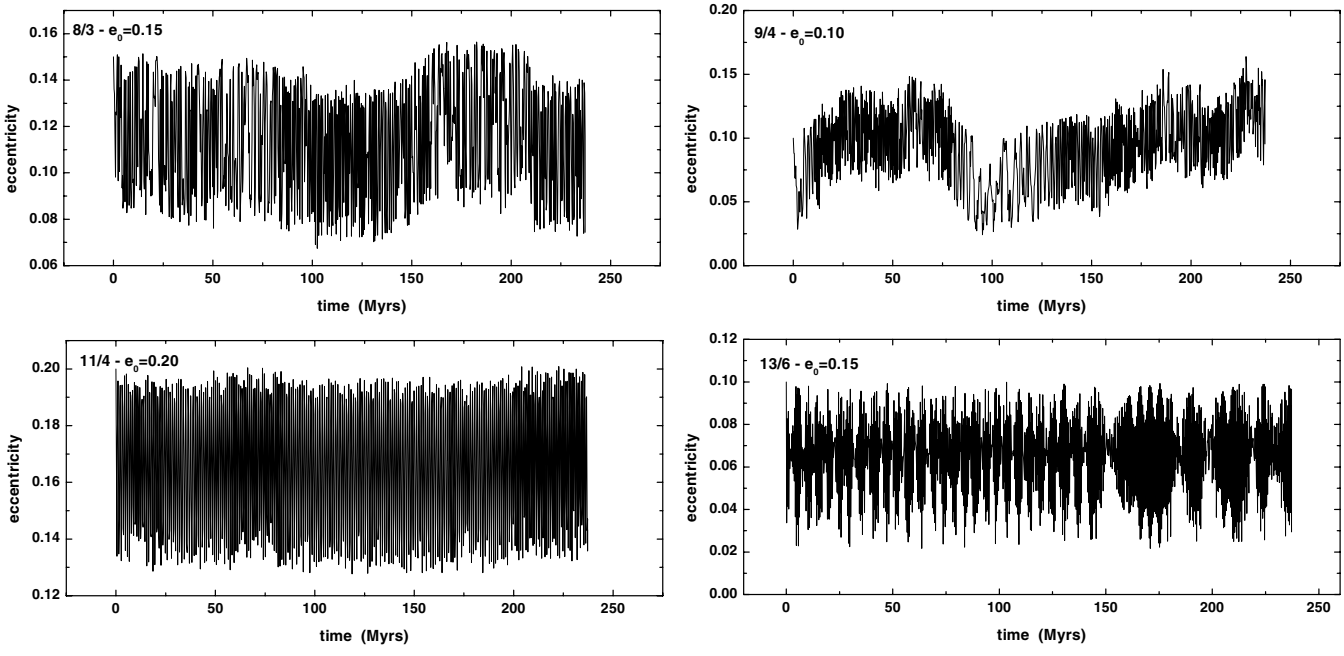

FIG. 6. The eccentricity evolution is shown for four RUN-I particles, started in the 8/3, 9/4, 11/4, and 13/6 resonances respectively. As the aforementioned resonances do not carry periodic orbits, a small-amplitude, diffusive, evolution of e is observed. The 13/6 orbit shown here is an example of stable chaos, as $e(t)$ retains linear correlations for $t \sim 100$ Myr (see Section 4.3).

TABLE II
Inner-Belt Escapers of RUN-II

$(p+q)/p$	e_0	Fate (3BP)	T_{MC}	T_{esc}	Fate (OSS)	T_{MC}	T_{esc}
4/1	0.05	→Sun	40.470	40.541	→Sun	0.283	9.420
	0.10	→Sun	10.130	10.202	→Sun	0.265	1.823
	0.15	→Sun	0.146	0.218	→Sun	0.295	6.728
7/2	0.15	—	—	—	→Sun	65.600	82.960
3/1	0.05	→Sun	7.400	64.035	→Sun	0.820	1.200
	0.10	→Sun	1.900	86.001	→Sun	0.760	3.660
	0.15	→Sun	2.600	85.260	→Sun	0.216	24.487
5/2	0.05	MC	0.246	—	→Jup	0.920	32.332
	0.10	MC	0.312	—	→Jup	0.130	16.503
	0.15	MC	0.042	—	→Jup	0.134	14.647
7/3	0.05	→Jup	86.045	153.068	→Jup	47.772	47.923
	0.10	→Jup	23.300	217.705	→Jup	73.577	74.135
	0.15	MC	19.400	—	→Jup	5.840	6.542
9/4	0.10	—	—	—	→Jup	118.700	118.972
	0.15	—	—	—	→Jup	167.720	169.244
2/1	0.05	→Sun	14.570	183.423	→Sun	63.850	96.485
	0.10	→Sun	205.904	206.399	→Sun	34.860	39.054
	0.15	—	—	—	→Sun	65.503	71.318

Note. The resonance ratio and the initial eccentricity of the test particle are given in the first two columns. The fate of the particle, where MC stands for Mars-crosser, is then shown. T_{MC} (in Myr) is the time at which the orbit first crosses the one of Mars, i.e., $q < 1.5$ AU, and T_{esc} (in Myr) is the time at which the orbit encounters either Jupiter or the Sun ($q < 0.005$ AU). The last three columns refer to the OSS integration. All escapers are Mars-crossers, so MC is written only for those that *do not* end up as Jupiter-crossers or Sun-grazers.

for reaching planet-crossing values may be much longer than 250 Myr. Note that there are no large differences in terms of T_L among the integrated particles, however, the escape time may vary by orders of magnitude. This result implies that the escape time depends more on the overall phase space structure near a given resonance than on the value of T_L.

We concentrate on the results of RUN-II. A summary of the results is given in Table I. In the 3BP model 42.0% of the integrated particles "escaped" from the belt. Outer-belt particles encountered Jupiter and were ejected on hyperbolic orbits. On the other hand, inner-belt particles attained Mars-crossing eccentricities and some of them reached a pericenter distance $q \leq 0.005$ AU, thus "falling" into the Sun. In the OSS integration the percentage of escapers increased, as expected, to 53.6%. None the less, half of the particles, despite the fact that most of them follow chaotic orbits as shown here, survived for 250 Myr. In the 3BP integration the only inner-belt particles that escaped were the ones started inside the gap resonances, i.e., the 2/1, 3/1, 4/1, 5/2, and 7/3 resonances. All these resonances, apart from the 7/3 one, carry resonant periodic orbits in the 2D elliptic problem. The peculiarity of the 7/3 resonance will become apparent in a following section. In the outer belt this correlation seems to be lost, as particles escape also from resonances that do not have periodic orbits. However, no particle starting near the 12/7 or the 13/8 resonance escaped. The OSS integration was not very different in terms of escaping particles. The gap resonances were evacuated. Three more inner-belt particles, two from the 9/4 region and one from the 7/2 region, escaped. In the outer belt three more escapers were also found (one from each of the 11/6, 11/7, and 3/2 resonances) but the 12/7 and 13/8 particles still survived for the entire integration time span. The fate of the "escapers" and the time of escape, T_{esc}, are given in Table II for inner-belt particles and in Table III for outer-belt particles. The fact that in the OSS model only a few more escapes are found, as well as the data concerning the escape time (Tables II and III), lead to the conclusion that the evolution of chaotic orbits is faster in the OSS model. However, for this set of small-eccentricity orbits no dramatic changes were detected, with respect to the 3BP behavior. This last remark holds for the "thin" resonances ($q \geq 4$).

The particles that survived the integration sum up to 58.0% in the 3BP model and 46.4% in the OSS model. For these orbits a set of time-averaged elements was computed, as an approximation to *proper elements*, which are quasi-integrals of motion. A time series for these averaged elements, a_P, e_P, and $\sin I_P$, was derived, using a running window (as in Tsiganis *et al.* 2001) of length N, corresponding to 10 Myr,

$$X_P(t_i) = \frac{1}{N} \sum_{j=i-N/2}^{i+N/2} X(t_j), \tag{2}$$

where X_P stands for any element. The variations of the values of the X_P's with time is an indicator of orbital stability. This can

TABLE III
Outer-Belt Escapers of RUN-II

$(p+q)/p$	e_0	T_{esc} (3BP)	T_{esc} (OSS)
11/6	0.10	119.856	78.452
	0.15	—	28.256
9/5	0.05	31.929	62.630
	0.10	33.976	14.804
	0.15	94.400	10.543
7/4	0.05	0.172	0.087
	0.10	0.016	0.014
	0.15	8.133	0.188
5/3	0.05	3.182	0.724
	0.10	1.041	1.358
	0.15	0.053	0.028
8/5	0.05	10.115	0.461
	0.10	8.800	2.452
	0.15	3.243	0.325
11/7	0.10	—	192.294
	0.15	39.945	43.666
3/2	0.05	54.221	8.472
	0.10	—	34.699
	0.15	47.910	6.928

Note. The resonance ratio, the initial eccentricity, and the time (in Myr) of encounter with Jupiter is given for each particle.

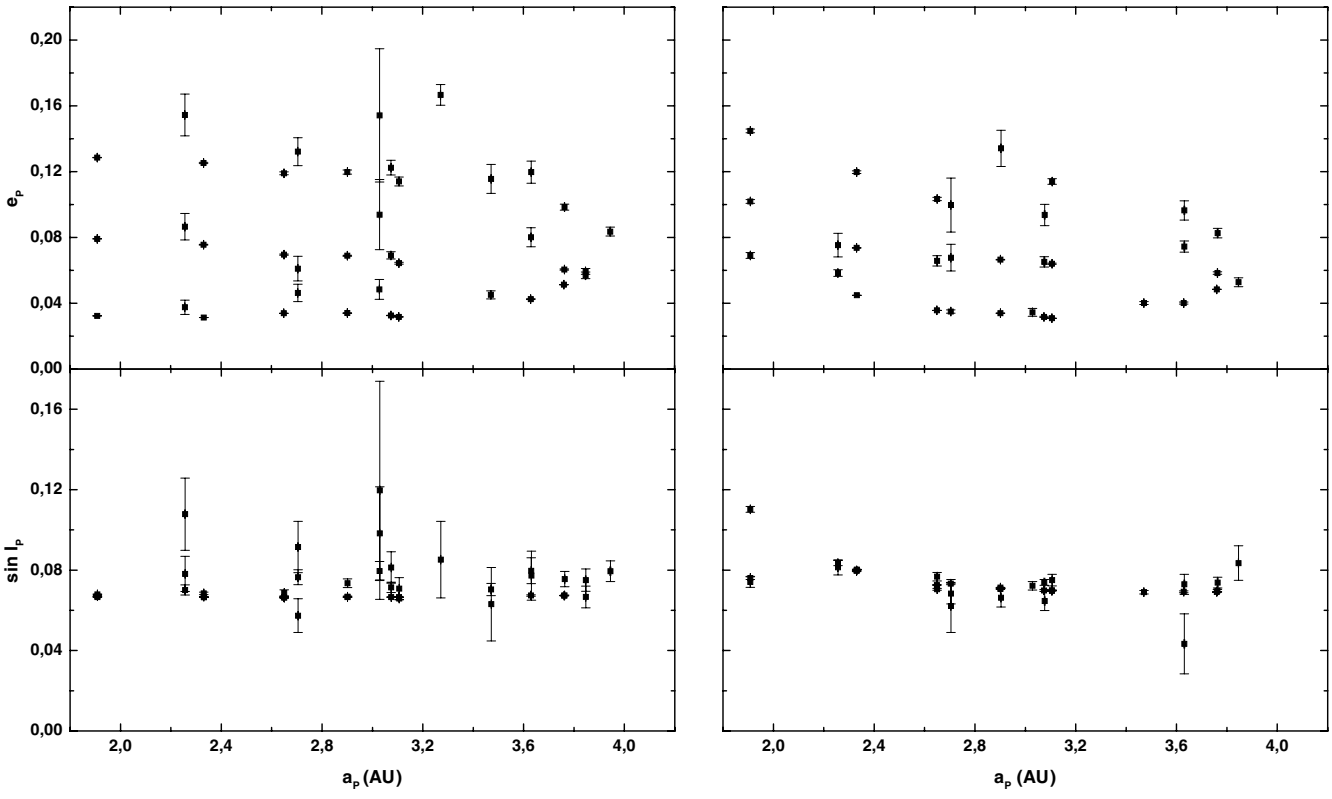

FIG. 7. The surviving particles of the RUN-II integrations are shown on the planes of the time-averaged elements (a_P, e_P) (top) and (a_P, $\sin I_P$) (bottom). The left panels are the results of the 3BP integration, and the right panels correspond to the OSS integration. Each particle is represented by a square, the coordinates of which are the mean values of the corresponding elements, X_P, and the superimposed error bars have a length equal to the respective value of $\sigma(X_P)$.

be quantified by means of the standard deviation of X_P,

$$\sigma(X_P) = \sqrt{\sum_{i=1}^{M} \frac{(X_P(t_i) - \langle X_P \rangle)^2}{M}}, \qquad (3)$$

where M is the number of points in the time series of the averaged element and $\langle X_P \rangle$ is the mean value of the averaged element. The results of these calculations are shown graphically in Fig. 7, where each of the remaining particles is represented by a point, the coordinates of which are the corresponding mean values of a_P, e_P, and $\sin I_P$. The error bars, superimposed on each point, have a length equal to the corresponding values of $\sigma(a_P)$, $\sigma(e_P)$, or $\sigma(\sin I_P)$. It is evident from this plot that there are two types of orbits surviving the integration, a feature common both to the 3BP and the OSS models. In the 3BP integration about half (48%) of the surviving orbits have $\sigma(e_P) < 0.005$, $\sigma(a_P) < 10^{-3}$ AU, and $\sigma(\sin I_P) < 10^{-3}$. The rest of the orbits show a tendency of becoming unstable, as the variations of e_P and $\sin I_P$ are larger. Only two orbits have $\sigma(e_P) > 0.01$ and five orbits have $\sigma(\sin I_P) > 0.01$. We remind the reader that almost all orbits are in fact chaotic with $T_L < 10^5$ years. In the OSS integration the percentage of orbits with $\sigma(e_P) < 0.005$ *increases* to 81% (26/32). Again, only two orbits have $\sigma(e_P) > 0.01$ (one of which also has $\sigma(\sin I_P) > 0.01$) and two orbits have $\sigma(\sin I_P) > 0.01$. Finally, almost all OSS surviving orbits have $\sigma(a_P) < 10^{-3}$ AU. We note that, for the survivors, e_P is more stable in the OSS integration. However, an orbit-by-orbit comparison should not be attempted. Mean motion resonances are not fixed in space in the OSS model. Furthermore, as osculating elements have additional quasi-periodic forced variations in the OSS model, an initial osculating value of e_0 corresponds a different value of e_P in each model.

4.3. Long-Time Correlated Motion—Stable Chaos

As already mentioned, the orbits of most of the nonescaping particles are chaotic. However, there appear to be two distinct types of chaotic motion. The difference is visible in the time evolution of the autocorrelation function, $r(t)$, of the Delaunay actions. As was first noted in Tsiganis *et al.* (2000, 2002), there exist chaotic orbits, which are the ones that we refer to as *stable-chaotic*, that have a very characteristic spectrum of autocorrelation times. The autocorrelation function $r_L(t)$ of the action conjugate to the mean longitude ($L = \sqrt{a}$) decays exponentially with time (as expected for a chaotic signal) on a time scale comparable to the Lyapunov time. On the other hand, $r_G(t)$ and $r_H(t)$, which are the autocorrelation functions of the eccentricity- and inclination-related Delaunay actions

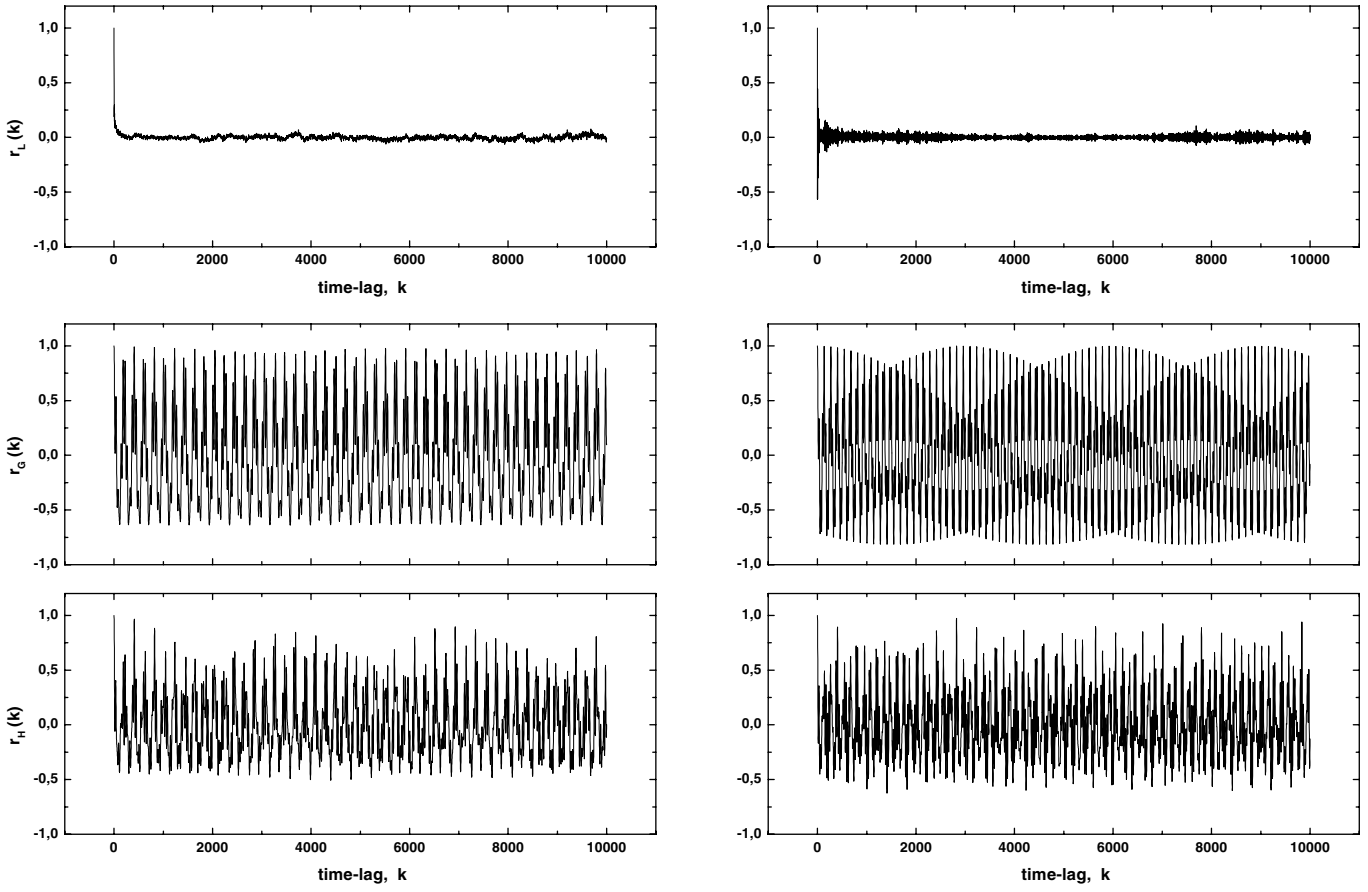

FIG. 8. The autocorrelation functions $r(t)$ for the three actions L, G, and H are shown (from top to bottom) as functions of time. The unit of the time lag, k, corresponds to 100 $T_J \approx 1200$ years. Two stable-chaotic orbits are shown in this figure. Note that $r_L(t)$ decays exponentially with time on a time scale comparable to $T_L \sim 10^4$ years. The other two actions have autocorrelation functions that vary almost quasi-periodically with time.

(respectively $G = L\sqrt{1-e^2}$ and $H = G\cos i$), show an extremely slow decay with time, retaining linear correlations for $t \gg T_L$ (often for $t > 10^3\, T_L$). In fact $r_G(t)$ and $r_H(t)$ seem to evolve in an almost quasi-periodic manner. As conjectured by Tsiganis *et al.* (2002), this picture is consistent with the near conservation of an additional, local, integral of motion. We note that this property does not hold for all cases of chaotic orbits that survive for a long integration time, and it can be used to distinguish between the *slow diffusion* predicted by the model of Murray and Holman (1997) and what we refer to as *stable chaos*.

Among the particles that survived in the OSS integration, both *slow* and *stable* chaos is present. The autocorrelation functions of all three actions are shown in Figs. 8 and 9 for four characteristic trajectories of different behavior. These plots were produced using the first 25 Myr of the osculating elements. Two stable-chaotic orbits are shown (Fig. 8), for which $r_L(t)$ decays fast while $r_G(t)$ and $r_H(t)$ are almost quasi-periodic functions of time. A slowly diffusing chaotic orbit, for which all $r(t)$'s decay exponentially with time on a very similar time scale, is shown in Fig. 9. Finally, intermediate cases can be found (Fig. 9), for which a strong quasi-periodic component and slowly decaying amplitudes of $r_G(t)$ and $r_H(t)$ are observed. We note that the orbits for which all three $r(t)$'s decay exponentially with time have the largest values for $\sigma(a_P)$, $\sigma(e_P)$, and $\sigma(\sin I_P)$.

4.4. The 7/3 Resonance

This resonance is a rather puzzling case. As seen in Section 3, no bifurcation point from which the periodic orbits of the circular problem can continue was found, either in the elliptic or in the 3D problem. Thus one can conclude that there is no "fast" mechanism of eccentricity transport in the 3BP model. However, the 7/3 particles integrated in the 3BP model, both in RUN-I and in RUN-II, did manage to become Mars-crossers. Moreover, as shown in Figs. 5 and 10, their eccentricity evolution shows an intermittent pattern, with jumps up to $e \approx 0.55$, a picture consistent with the existence of an island of libration. The same initial conditions were used in a more accurate Bulirsch–Stoer integration, and the results remained the same. For this reason we decided to perform another integration (in both models) of 24 test particles set initially in the 7/3 resonance on an 8×3 grid in the (a, e) space, with $2.9515 \le a \le 2.9605$ AU and $e = 0.05, 0.1$, and 0.15. The rest of the orbital elements, as well as the integration

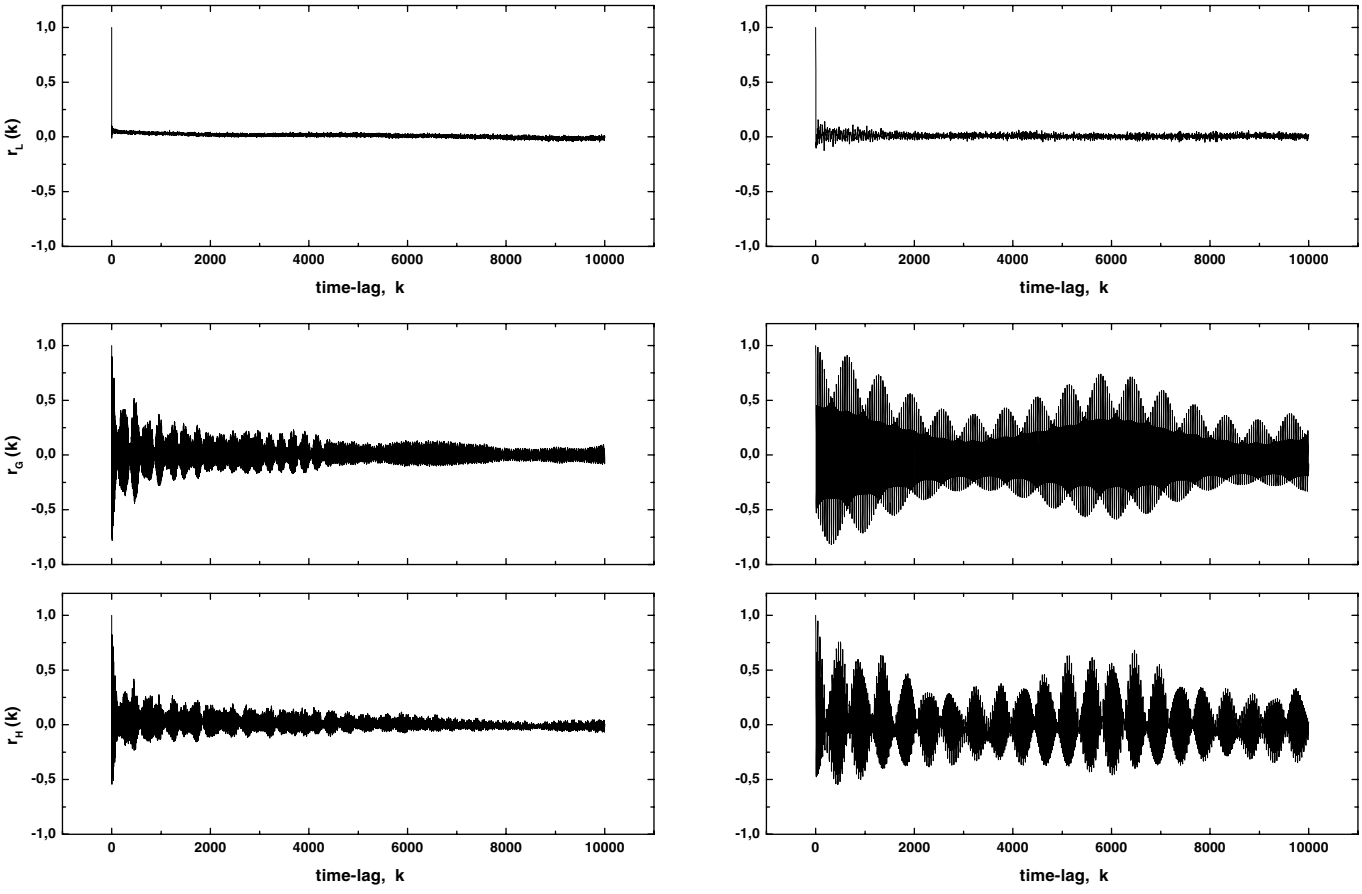

FIG. 9. The same as in Fig. 8, but for two different chaotic orbits. The left panel shows a slowly diffusing chaotic orbit, for which all three autocorrelation functions decay exponentially on a similar time scale. The right panel shows an intermediate case, where the amplitudes of $r_{\rm G}(t)$ and $r_{\rm H}(t)$ decay slowly, while a strong quasi-periodic component persists.

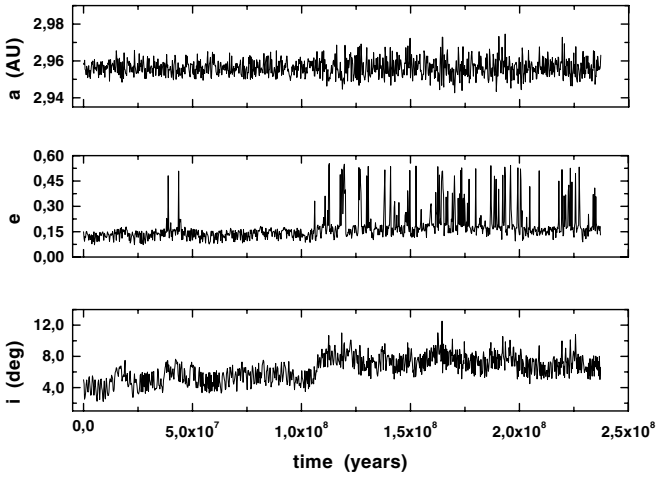

FIG. 10. The time evolution of a, e, and i for a 7/3-resonant orbit with $e_0 = 0.15$, in the 3BP model. Note the intermittent behavior of e. This behavior is accompanied by larger variations of a about $a_{\rm res}$ and also by a higher mean value of i, as seen on the plots.

parameters, were given the same values as in RUN-II. Checking the critical argument, $\sigma = 3\lambda - 7\lambda' + 4\varpi$, we verified that most of the particles again followed chaotic orbits.

In the 3BP integration 13 particles (54%) became Mars-crossers, 6 of which encountered Jupiter before the end of the integration. All of these orbits presented the same intermittent eccentricity behavior as in the previous runs. Figure 11 shows the projection of such an orbit on the $(\phi = \varpi - \varpi_{\rm J}, e)$ plane. The picture reveals the existence of an island of libration, associated with a stable periodic orbit centered at $e \approx 0.4$, $\phi = \pi$. The number of Mars-crossers increased to 14 (58.3%) in the OSS integration, all of which encountered Jupiter. The inclusion of more perturbing planets speeds up the evolution of chaotic orbits significantly. What is more important, though, is that the evolution of the orbital elements is quite different. Secular resonances (the ν_5 and ν_6) are now responsible for the growth of the eccentricity (see Fig. 12).

The question of course still remains as to why we were not able to detect the bifurcation point. We note that the stability index of the family of periodic orbits of the 2D problem shows a peak of $\mathrm{tr}(\mathbf{A}) = 1.99965$ at $e \approx 0.37$, i.e., very close to the value

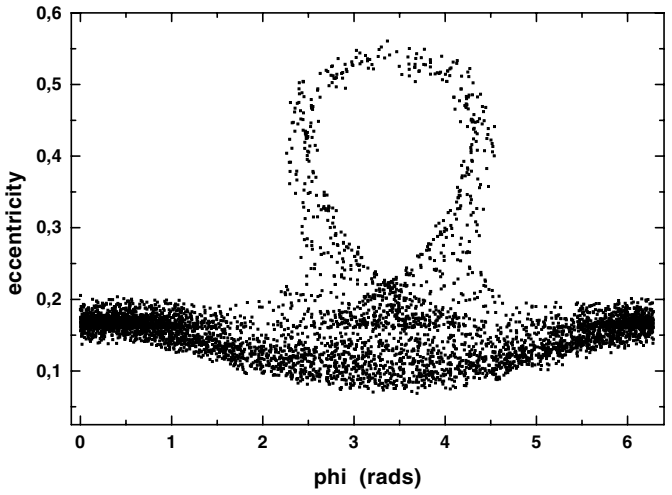

FIG. 11. A projection of the orbit shown in Fig. 10 on the (ϕ, e) plane. It is clear that the intermittent jumps in e are related to the libration island, centered at $e \approx 0.4$, $\phi = \pi$.

of e at which the periodic orbit seems to be located (Fig. 11). We are quite confident though that the curve does not intersect the $\mathrm{tr}(\mathbf{A}) = 2$ line, as the calculations were performed at an accuracy of 10^{-14}. By increasing the mass of Jupiter and recalculating the periodic orbits, we found that the situation becomes worse, as the maximum value of $\mathrm{tr}(\mathbf{A})$ decreases. The apparent inconsistency between our numerical results for the 7/3 resonance and the study of periodic orbits (Section 3) leads us to consider the possibility of this being a phenomenon that we did not take into account before. As a test, we integrated another set of 24 particles, with the same initial values for a, e, ϖ, and σ as before, but on the same plane as Jupiter. The difference between the 3D case and the co-planar one turned out to be remarkable. Although most of the orbits remained chaotic, none presented an intermittent

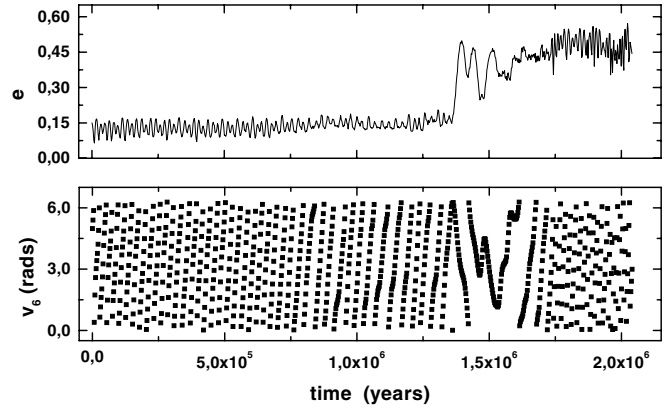

FIG. 12. Evolution of a 7/3-resonant orbit, starting with $e_0 = 0.15$ in the OSS model. No intermittent jumps are observed in the eccentricity time series. The large jumps of e, and subsequent escape, are correlated with the libration/circulation of the ν_6 secular resonant argument, $\nu_6 = \varpi - \varpi_S^*$, where $\varpi_S^* = g_6 t + \varpi_{S,0}^*$ is a linear approximation of Saturn's perihelion longitude.

eccentricity evolution and no Mars-crossers were found within 250 Myr. Almost all orbits had quite small variations in both a_P and e_P. Therefore, the intermittency seen before is clearly a 3D phenomenon. Thus, no bifurcation point exists and the periodic orbit seen in the numerical results must belong to an *irregular family*, i.e., a family of 3D periodic orbits that do not bifurcate from the $i_P = 0^\circ$ plane. This claim is supported by Fig. 13, where an intermittent orbit is projected on the (ϕ, e) plane, by splitting the data into two parts, (i) for $i \le 6^\circ$ and (ii) for $i > 6^\circ$. It is clear that the orbit is semiconfined within a small region of the (ϕ, e) plane when the inclination is small, while it escapes to much larger values of e only if the inclination is large enough.

A resonant periodic orbit occurs when all angles, σ, ϕ, and $\theta = \Omega - \Omega_J$ (in the 3BP), are stationary. In the three-body problem a periodic orbit coincides with the secular resonance

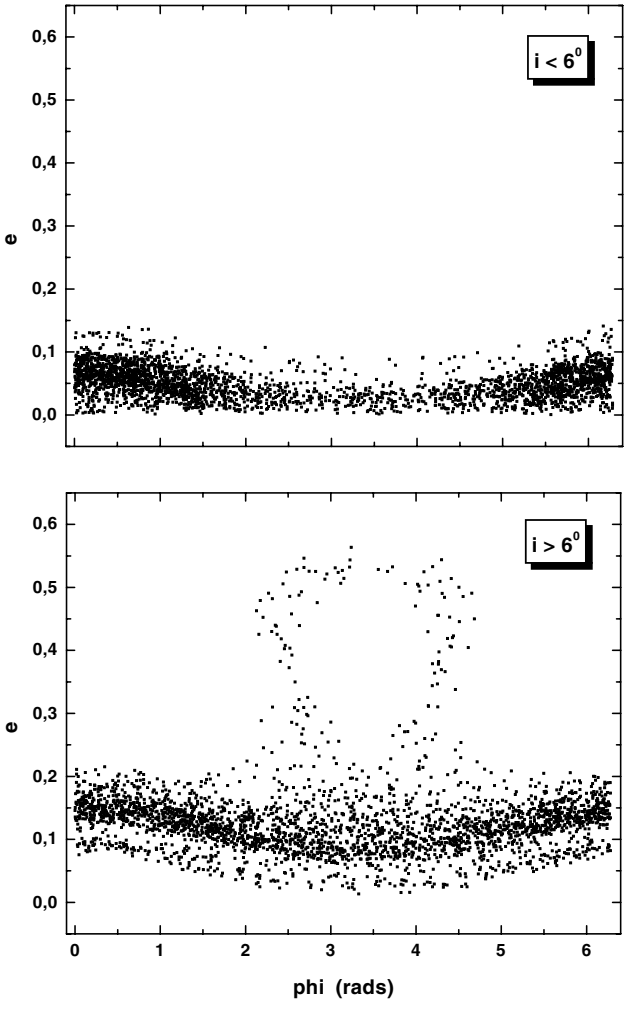

FIG. 13. Projection of another 7/3-resonant orbit on the $(\phi = \varpi - \varpi_J, e)$ plane (3BP model). If we split the data in two parts according to the value of the inclination, we see that the behavior is different for $i < 6^\circ$ than for $i > 6^\circ$. On the top panel ($i < 6^\circ$), the orbit explores a small region of the plane, defined roughly by $e < 0.15$. When $i > 6^\circ$ (bottom), chaotic wandering around the libration island forces the eccentricity to reach values up to 0.6.

$g = s = 0$. In the absence of resonance among the fast angles the frequencies $g \neq 0$ and $s \neq 0$ are determined by secular theory for different values of a, e, and i. Therefore, to have a periodic orbit, the mean motion resonance must be strong enough to modify g and s so that they become zero at some point(s) in the (a, e, i) space. For the lowest order (i.e., stronger) 2/1, 3/1, 4/1, and 5/2 resonances the condition $g = 0$ is found to hold for some co-planar orbits (the node is not defined) and these are the periodic orbits that are continued from the circular problem. This is not true for the 7/3 and most of the higher order resonances. However, the condition $g = s = 0$ may be fulfilled at higher values of i. This is what we observe in the 7/3 case. Thus, periodic orbits may also exist for higher order resonance ratios, but these orbits must be located at high inclinations (probably $i > 15°$).

4.5. A Note on the 3/2 Resonance and the Hilda Group

Most of the particles that we set initially in this resonance escaped (2/3 in the 3BP and 3/3 in the OSS model). As a group of resonant asteroids (the Hildas) is known to reside in this resonance, this outcome may seem strange. We note, however, that the 3/2 resonance is a first-order resonance of width in a that is quite large. The small number of particles set in resonance is not representative, especially since they were selected on purpose to be in the chaotic zone close to the resonance inner border. Several papers have been devoted to the dynamics of the 3/2 resonance and the apparent contradiction between the existence of the 3/2 resonant group and the 2/1 Hecuba gap (see Lemaitre and Henrard 1988, Nesvorný and Ferraz-Mello 1997, Ferraz-Mello *et al.* 1998; also see Moons 1997). Hadjidemetriou and Voyatzis (2000) found that a large part of the phase space, larger than in the 2/1 resonance, leads to chaotic motion in the 3/2 resonance. However, as their results show, secondary resonances do not overlap completely, in contrast to the 2/1 case, and a large number of chaotic orbits is expected to be "trapped" in the libration island of this resonance. In this respect, many Hildas may be thought of as *stable-chaotic* asteroids.

Instead of exploring this resonance by integrating the orbits of fictitious asteroids we decided to integrate the orbits of the real Hildas. The initial conditions of 144 objects were taken from the AstDys database.[5] In the same database a catalogue of proper elements and Lyapunov exponents, calculated by Knežević and Milani (2000), can also be found. As shown by these data, a large number of Hildas follow chaotic orbits. We verified this result by performing a 4-Myr integration (OSS model) of the variational equations (Fig. 14). Forty-nine Hildas (34%) have $T_L \leq 4 \times 10^5$ years. We integrated the orbits of these objects for 100 Myr into the future. Asteroid 19752 was found to encounter Jupiter by the end of the integration ($T_{\rm esc} \approx 96.4$ Myr). Apart from this case of hyperbolic escape, the computations of the time-averaged elements show that the rest of the particles are quite stable, having $\sigma(a_{\rm P}) \sim 10^{-4}$ AU, $\sigma(e_{\rm P}) \sim 5 \times 10^{-4}$, and $\sigma(\sin I_{\rm P}) \sim 5 \times 10^{-4}$. Based on these results one may be tempted to label the Hildas as examples of stable chaos. Calculations of the autocorrelation functions of the actions show that most of the Hildas are in fact diffusing, but at a very slow pace. We note that the phase-space geometry in the vicinity of the 3/2 resonance is very different from the high-order cases studied before. The basic topological feature in this case is the wide island of libration, and the Hildas are semiconfined *inside* this island. Thus the diffusion process by which chaotic Hildas can escape is probably very different from the one observed in high-order resonances (described by Tsiganis *et al.*, 2002) and further study of this behavior should be made.

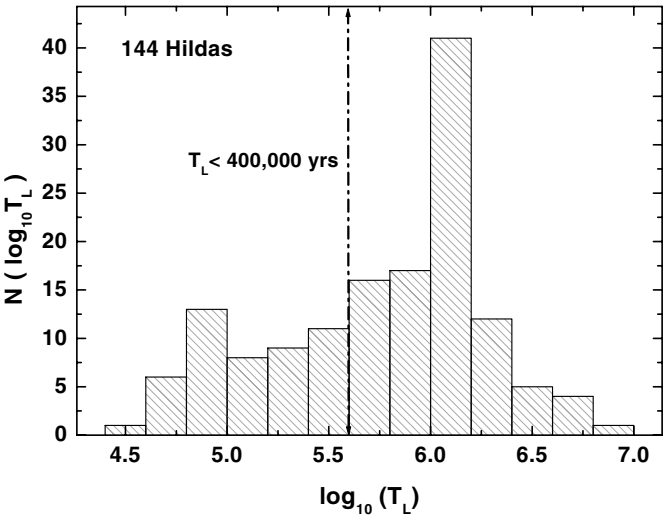

FIG. 14. Histogram of $\log T_{\rm L}$ for the 144 Hildas, integrated in the OSS model. Forty-nine objects are concentrated to the left of the vertical line, which marks the $T_{\rm L} = 4 \times 10^5$ years border.

5. CONCLUSIONS

We will now try to answer the question that we posed in the Introduction of this paper. In our first numerical experiment (RUN-I) we have seen that a fraction of ~10% of test particles placed inside the 3BP "belt" followed chaotic orbits, due to the action of the main mean motion resonances with Jupiter, typically with $T_{\rm L} < 2 \times 10^5$ years. In RUN-II we found that higher order resonances also lead to chaotic motion, with $T_{\rm L} < 10^5$ years. In particular we have seen, during our test integrations, that chaos is the typical orbital behavior in medium/high-order resonances, at least for orbits starting with $e_0 \geq 0.1$. Thus, even in the three-body problem, the volume of phase space covered by chaotic solutions is appreciable. However, many of these trajectories have orbital elements that are remarkably stable. We will attempt to explain this contradiction, by trying to understand which of the chaos-generating mechanisms (described in Section 2) act on each one of the 34 resonances studied in this paper.

In the inner asteroid belt ($1.9 \leq a \leq 3.3$ AU) a total of 21 resonances of order $1 \leq q \leq 9$ exist. Apart from the "gap resonances"

[5] http://hamilton.dm.unipi.it/astdys.

(2/1, 3/1, 4/1, 5/2, and 7/3), none of the rest carries periodic orbits. The 7/3 is the only resonance for which a possible irregular family of periodic orbits was detected. We cannot exclude the possibility of having resonant periodic orbits for other commensurabilities, but these orbits must be located at high inclinations. The existence of resonant periodic orbits leads to fast, intermittent eccentricity transport, as we have also seen in our numerical results. The word "fast" is only used in contrast to the "slow," diffusive evolution which takes place in the vicinity of resonances that do not carry periodic orbits. The actual time needed for an asteroid to escape from a gap resonance may be quite long, and the percentage of orbits that lead to escape may be small compared to the width of the libration zone of the resonance. The escape time is controlled by the period of secular evolution in the resonance, as this period defines the time needed for an orbit to travel around the island of libration of $\phi = \varpi - \varpi_J$. Furthermore, the escape time also depends on the initial eccentricity of the asteroid as well as on the distance of the resonance from a major planet, since the planet-crossing value of e is approximately given by $e_c = |a_{res} - a'|/a'$. Of course, the overlapping among the resonant harmonics further enhances chaotic transport inside the resonances that carry periodic orbits. In the remaining 16 resonances studied in this paper, which do not carry periodic orbits, chaos is solely generated by the overlapping of the harmonics of the resonance multiplet. No escapes were found in the 250-Myr 3BP integration and, moreover, the orbital elements of chaotic orbits are, in general, remarkably stable. From the results presented in Tsiganis *et al.* (2002), one can infer that this picture also holds for resonances with $q > 9$. According to the analytic theory of Murray and Holman (1997), which is valid for resonances that *do not* carry periodic orbits, the escape time for orbits starting from inner-belt resonances with $q > 5$ and $e_0 \sim 0.1$ should be longer than the age of the Solar System. Remember that this will be the case if resonance overlap among the terms of the multiplet is complete, i.e., the whole eccentricity axis is connected. If not, something which is expected to be rather common, semiconfined chaotic motion (i.e., stable chaos), will also occur. Many orbits of this kind, which are characterized by a nearly quasi-periodic evolution of e and i for extremely long times, were also found in our integrations.

As an overall evaluation of our results for the inner belt, we can conclude that there exists a correlation between gaps in the distribution of asteroids and resonances that carry periodic orbits. Imagine a simplified model of our planetary system, consisting of the Sun, a Jupiter-like ($\mu \sim 1/1000$) planet, and a disk of small bodies, inner to the planet. As shown in our results, the resonances in which the Kirkwood gaps are presently observed are the only resonances inner to the 11/6 that have the ability to sculpt gaps in the small-body disk, at least for times comparable to the lifetime of our Solar System. This is because only these resonances can force asteroids to develop planet-crossing or Sun-grazing orbits on a time scale of ~100 Myr. Of course, complete evacuation of these gaps would not occur, since secular resonances (i.e., more planets) are needed to destroy the stability islands and enhance eccentricity transport for a much larger volume of initial conditions. In this three-body model, as our results show, the majority of resonances would be inefficient in creating gaps, at least for orbits starting in the small-eccentricity and small-inclination region ($e < 0.15$, $i \leq 15°$). If more perturbing planets are taken into account, the effect of medium/high-order mean motion resonances (with no periodic orbits) would not be very different from the 3BP model. This means that the pulsation of resonances, induced by the precession of Jupiter's orbit, does not enhance significantly the overlap among the terms of a resonant multiplet. Also, because $q \geq 3$, these resonances are too "weak" to significantly modify the values of the secular frequencies, with respect to those predicted by secular theory. Thus, secular resonances do not occur inside these resonances either. Therefore, the existence of a significant number of resonant asteroids on slowly diffusing, or even stable-chaotic, orbits should not be a surprise.

For the outer-belt resonances, the role played by periodic orbits is not so clear. The theory of Murray and Holman (1997) predicts that the escape time, due to diffusive chaos, can be very small. The diffusion rate depends on the order of the resonance and the initial value of the asteroid's free eccentricity. In fact orbits with $e_0 \sim 0.1$ can become Jupiter-crossing within 10^8 years in most of the resonances studied. The 7/4, 5/3, and 8/5 resonances should be the most efficient ones, and this is also shown in our results. Especially for the 7/4 and 5/3 cases, resonant periodic orbits were also found to exist. However, the overlap among the terms of the resonant multiplet is certainly exhaustive in these two resonances. Taking into account that adjacent resonances also begin to overlap at $e > 0.15$, we can understand why most of the orbits starting from the vicinity of the 7/4 and 5/3 resonances should cross Jupiter's orbit within less than 1 Myr. Thus, the fact that periodic orbits do exist for these resonances may be of no significance at all, since the stability island is probably destroyed and its associated chaotic layer could not be viewed separately from the large, connected, chaotic sea. On the other hand, higher order resonances, such as the 12/7 and 13/8, have a characteristic escape time which is $\sim 10^9$ years for $e \sim 0.1$. Since no other transport mechanism (i.e., periodic orbits) exists for the 12/7 and 13/8 cases, no escape within a 250-Myr integration should be expected, and this is what we actually observed. When all outer planets are included, eccentricity transport in the outer belt is also enhanced. There are, however, still regions, like the 12/7 resonance, where *stable chaos* persists (see Tsiganis *et al.* 2000).

ACKNOWLEDGMENT

K. Tsiganis wishes to acknowledge financial support by the State Scholarship Foundation of Greece (IKY).

REFERENCES

Bretagnon, P. 1974. Termes à longues périodes dans le système solaire. *Astron. Astrophys.* **30**, 141–154.

Ferraz-Mello, S., T. A. Michtchenko, D. Nesvorný, F. Roig, and A. Simula 1998. The depletion of the Hecuba gap vs. the long-lasting Hilda group. *Planet. Space Sci.* **46**, 1425–1432.

Hadjidemetriou, J. D. 1993. Resonant motion in the restricted three-body problem. *Celest. Mech. Dynam. Astron.* **56**, 201–219.

Hadjidemetriou, J. D., and G. Voyatzis 2000. The 2/1 and 3/2 resonant asteroid motion: A symplectic mapping approach. *Celest. Mech. Dynam. Astron.* **78**, 137–150.

Henrard, J., and N. D. Caranicolas 1990. Motion near the 3/1 resonance of the planar elliptic restricted three body problem. *Celest. Mech. Dynam. Astron.* **47**, 99–121.

Holman, M., and N. Murray 1996. Chaos in high-order mean motion resonances in the outer asteroid belt. *Astron. J.* **112**, 1278–1293.

Knežević, Z., and A. Milani 2000. Synthetic proper elements for outer main belt asteroids. *Celest. Mech. Dynam. Astron.* **78**, 17–46.

Knežević, Z., A. Milani, P. Farinella, Ch. Froeschlé, and C. Froeschlé 1991. Secular resonances from 2 to 50 AU. *Icarus* **93**, 316–330.

Laskar, J. 1990. The chaotic motion of the Solar System: A numerical estimate of the size of the chaotic zones. *Icarus* **88**, 266–291.

Lemaitre, A., and J. Henrard 1988. The 3/2 resonance. *Celest. Mech. Dynam. Astron.* **43**, 91–98.

Levison, H. F., and M. J. Duncan 1994. The long-term dynamical behavior of short-period comets. *Icarus* **108**, 18–36.

Michel, P., F. Migliorini, A. Morbidelli, and V. Zappalà 2000. The population of Mars-crossers: Classification and dynamical evolution. *Icarus* **145**, 332–347.

Milani, A., and A. M. Nobili 1992. An example of stable chaos in the Solar System. *Nature* **357**, 569–571.

Milani, A., A. Nobili, and Z. Knežević 1997. Stable chaos in the asteroid belt. *Icarus* **125**, 13–31.

Moons, M. 1997. Review of the dynamics in the Kirkwood gaps. *Celest. Mech. Dynam. Astron.* **65**, 175–204.

Moons, M., and A. Morbidelli 1995. Secular resonances inside mean-motion commensurabilities: The 4/1, 3/1, 5/2 and 7/3 cases. *Icarus* **114**, 33–50.

Morbidelli, A., and M. Guzzo 1997. The Nekhoroshev theorem and the asteroid belt dynamical system. *Celest. Mech. Dynam. Astron.* **65**, 107–136.

Murray, N., and M. Holman 1997. Diffusive chaos in the outer asteroid belt. *Astron. J.* **114**, 1246–1259.

Murray, N., M. Holman, and M. Potter 1998. On the origin of chaos in the asteroid belt. *Astron. J.* **116**, 2583–2589.

Nautical Almanac Office, U.S. Naval Observatory 2001. *The Astronomical Almanac*, U.S. Government Printing Office, Section E3.

Nesvorný, D., and S. Ferraz-Mello 1997. On the asteroidal populations of the first order jovian resonances. *Icarus* **130**, 247–258.

Nesvorný, D., and A. Morbidelli 1998a. Three-body mean motion resonances and the chaotic structure of the asteroid belt. *Astron. J.* **116**, 3029–3037.

Nesvorný, D., and A. Morbidelli 1998b. An analytic model of three-body mean motion resonances. *Celest. Mech. Dynam. Astron.* **71**, 243–271.

Nobili, A. M., A. Milani, and M. Carpino 1989. Fundamental frequencies and small divisors in the orbits of the outer planets. *Astron. Astrophys.* **210**, 313–336.

Šidlichovský, M. 1999. On stable chaos in the asteroid belt. *Celest. Mech. Dynam. Astron.* **73**, 77–86.

Tsiganis, K., H. Varvoglis, and J. D. Hadjidemetriou 2000. Stable chaos in the 12 : 7 mean motion resonance and its relation to the stickiness effect. *Icarus* **146**, 240–252.

Tsiganis, K., H. Varvoglis, and J. D. Hadjidemetriou 2002. Stable chaos in high-order jovian resonances. *Icarus* **155**, 454–474.

Wisdom, J. 1982. The origin of the Kirkwood gaps: A mapping for asteroidal motion near the 3/1 commensurability. *Astron. J.* **87**, 577–593.

Wisdom, J., and M. Holman 1991. Symplectic maps for the n-body problem. *Astron. J.* **102**, 1528–1538.